Simultaneous Ultrasonic Evaluation with Differentiation of Stress and Texture

J.F. Smith and R.B. Thompson

An ultrasonic method for either independent or simultaneous determination of stress and texture is discussed. Quantitative differentiation between stress and texture during simultaneous measurements can be made. The method is useful for unidirectionally rolled, extruded, or cast material, and the validity of the method has been experimentally verified by extensive tests on rolled materials. Electromagnetic acoustic transducers (EMAT's) have been used, and these allow measurements during processing. In principle the method is applicable to non-conducting materials if piezoelectric or ferroelectric transducers are used, but since they are contracting and EMAT's are noncontacting, the constraints are more severe.

Keywords
sheet metal, stress, texture, ultrasonics

1. Introduction

THIS investigation is concerned with the ultrasonic measurement and quantitative evaluation of stress levels and the degree of preferred grain orientation in polycrystalline sheet and plate. Ultrasonic techniques are rapid, nondestructive, relatively inexpensive, and provide bulk information for the volume sampled by the ultrasonic wave. This contrasts with x-ray and neutron diffraction techniques for both stress and texture determination, where coupons must be cut and measurements are slow. In addition, x-ray techniques for both stress and texture are primarily surface measurements; likewise, strain gages measure only surface distortion. Neutron diffraction is capable of measuring bulk properties, but is slow, costly, nonportable, and destructive. Finally, ultrasonic techniques can be readily automated, allowing measurements to be made while material is being processed (e.g., dynamic measurements of texture in material exiting a rolling mill).

Although this discussion is concerned primarily with unidirectionally rolled sheet and plate, obviously some aspects of the findings presented here are applicable in other contexts. Ultrasonic measurement while distinguishing between stress and texture in unidirectionally rolled material is based on the premise that the material being tested has orthorhombic symmetry when in an unstressed condition. Justification for approximating unidirectionally rolled polycrystalline material as pseudo-orthorhombic is based on the fact that, during rolling reduction, equal stresses operate on the top and the bottom of the material—so there is no resultant difference in bias of granular orientation between the top and bottom. Thus, the granular orientation produced by the deformation should be mirrored in the horizontal plane. Secondarily, although rolling will produce preferred orientations in the rolling direction, there is an equal a priori probability that the granular deformation will produce orientations with the same number of grain axes oriented toward the left as to the right. Therefore, there should be a pseudo-mirror oriented vertically along the rolling direction. The symmetry of two orthogonal mirrors necessitates a third mutually orthogonal mirror so that the overall symmetry is pseudo-orthorhombic.

The velocities of acoustoelastic waves in an orthorhombic material vary with direction and polarization of propagation.

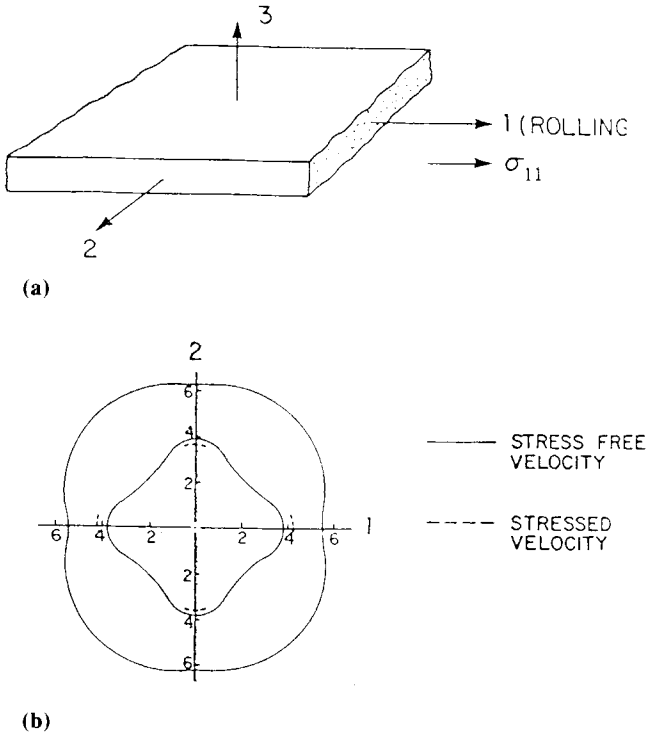

Fig. 1 (a) Orientation of a rolled sheet of a hypothetical material. (b) Angular dependences of the velocities of longitudinal waves (outer curve) and shear waves (inner curves). The solid lines represent the unstressed condition. The dashed segments illustrate the relative magnitude of expected changes for the important directions of shear-wave propagation.

J.F. Smith and **R.B. Thompson,** Ames Laboratory, U.S. Department of Energy and Department of Materials Science and Engineering, Iowa State University, Ames, IA 50010, USA

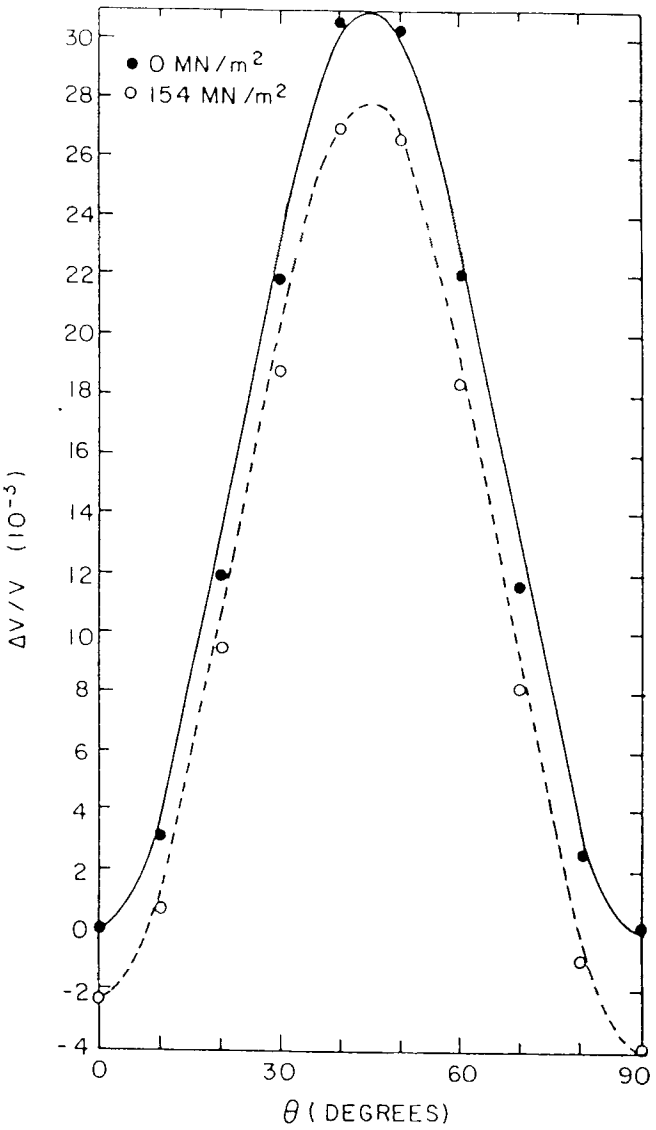

Fig. 2 Angular dependence of the relative velocities of a horizontally polarized shear wave in a rolled copper sample in an unstressed state (solid data points) and in a stressed state (open data points). 0° represents the rolling direction, and 90° represents the transverse direction. The V in the denominator of the ordinate is the wave velocity for propagation in the 0° direction in the unstressed state.

Figure 1 shows a plot of velocities as a function of propagation direction in the rolling plane for a unidirectionally rolled hypothetical material. The outer ring represents the directional variation of the bulk longitudinal mode, and the inner ring represents the directional variation of the shear mode polarized in the rolling plane. The solid lines are complete contours for unstressed material. The dashed lines represent partial contours near the rolling and transverse directions that indicate how a stress field affects the shear-wave velocities differently in different directions. As noted later, the presence of a stress tends to lower symmetry, and Fig. 1(b) shows that stress lifts the degeneracy of two orthogonally propagated shear waves whose polarizations are in their mutually shared plane.

2. Ultrasonic Waves and Stress

For a small-amplitude acoustoelastic wave propagating through an unstressed material, a combination of Hooke's law and Newton's law generates the relationship (Ref 1):

$$\rho V^2 = f(C_{ij}) \quad \text{(Eq 1)}$$

where $f(C_{ij})$ is a function of the elastic constants of the medium and depends on the type of wave and on the directions of propagation and polarization, ρ is the density of the material, and $V = \{f(C_{ij})/\rho\}^{1/2}$ is the velocity of propagation. If the material is under the influence of a stress field, the velocity equation must be modified (Ref 2-4) to include the stress tensor, T:

$$\rho V'^2 = f(C'_{ij}) + g(T_{ij}) \quad \text{(Eq 2)}$$

where the C'_{ij} are effective elastic constants, as modified by strain. Thus, the C'_{ij} are slightly shifted from the C_{ij} because of the stress-induced strain and satisfy the symmetry relations dictated by the combination of the pseudo-orthorhombic material symmetry and the symmetry implied by the applied stress. To lowest order (all that is generally needed), g is a linear function of the T_{ij}. Because the shifts in the effective elastic moduli are proportional to the stress-induced strain, Eq 2 can be linearized to the form:

$$V' - V) = kT \quad \text{(Eq 3)}$$

where k is known as the acoustoelastic constant and subscripts are suppressed for conceptual simplicity. Thus, the net stress within a material can be determined by the velocity difference between the stressed and unstressed states.

Figure 2 shows experimental data for the relative shift in the velocity of a shear wave with horizontal polarization in the rolling plane of a copper sheet. The relative velocity is plotted as a function of propagation angle with respect to the rolling direction. The V in the denominator of the ordinate of the plot is the unstressed velocity along the 0° direction of propagation. An example of the practical utilization of the relationship given in Eq 3 is the determination of bolt tension (Ref 5). The case of bolt tensioning is a particularly simple example, because the velocity can be measured in the initial untensioned state and can be monitored as tension is changed.

It is more generally desired to measure the stress in a material already under load, so the initial $f(C_{ij})$ are not directly measurable. The measurement can still be accomplished by combining two or more independent measurements. The simplest approach (Ref 6) is to measure the velocities of two shear waves propagated orthogonally with polarizations in the plane defined by the two propagation directions. Two such waves induce identical strains as they pass through the material, and, in a stress-free material, their velocities are degenerate. In a material under a state of anisotropic stress, however, a difference between the two velocities is a measure of a difference between the stress levels in the two directions. The nature of the wave propagation is shown in Fig. 3(a), and an application of this

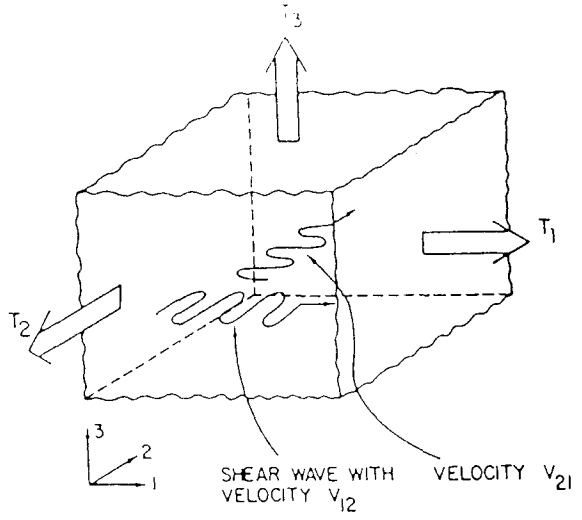

(a)

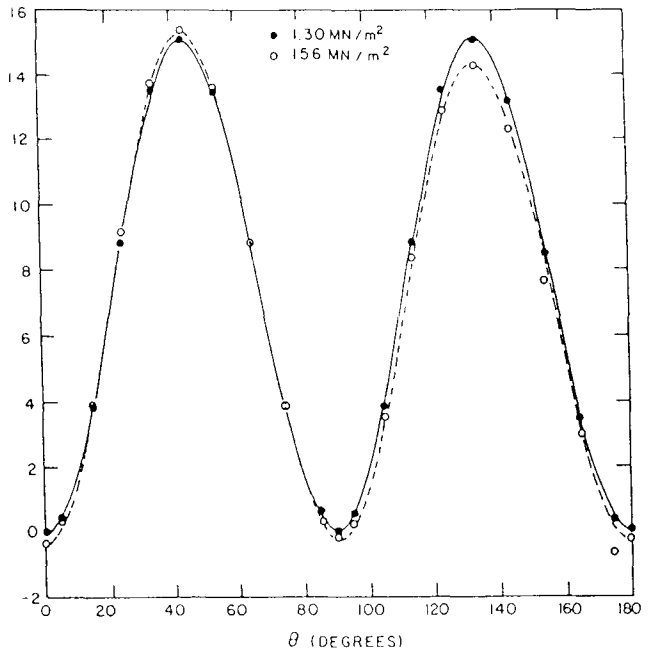

(b)

Fig. 3 (a) Degenerate waves in an unstressed orthorhombic material. (b) Angular dependence of the relative velocities of shear waves with polarization in the rolling plane in an essentially unstressed state (solid data points) and with an applied stress 45° from the rolling direction (open data points). The definitions of numerical angle and of V are the same as in Fig. 2.

type of wave propagation is shown in Fig. 3(b), where data from the rolling plane in a unidirectionally rolled sheet of type 304 stainless steel are plotted for both the stressed and the unstressed states. Again, the V in the denominator of the ordinate is the velocity of propagation along the rolling direction in the unstressed state, and 0° is the rolling direction. Here stress was applied 45° from the rolling direction. The presence of a stress in this direction is obvious from the difference in the relative velocities between 45° and 135° in the stressed state.

The question then becomes one of quantifying the difference to evaluate the magnitude of the stress level. The present authors were involved with a series of papers (Ref 4, 6-11) that addressed this problem through utilization of the general theory of acoustoelasticity developed by Tokuoka and Iwashimizu (Ref 12). King and Fortunko (Ref 13, 14) and Man and Lu (Ref 15) have undertaken related work. The present authors' approach considered that the stresses of interest in sheet and plate are the principal stresses lying in the plane of the plate (the 1-2 plane of Fig. 1). Within this 1-2 plane, the directions shown in Fig. 4 may be used to define the problem of evaluation of the resultant stress when the stress field is oriented in an arbitrary direction and no measurement of the elastic behavior in the unstressed condition is available. The results that were derived show that the velocity, V_T, of a shear wave polarized in plane and propagating in an arbitrary direction, Θ, should conform to the relationship (Ref 4):

$$\rho V_T^2 = T + C_T + \left(\frac{\beta C_T}{2}\right)(1 - \cos 4\Theta) - \left(\frac{\beta^2}{4}\right)\left(\frac{C_T^2}{C_L - C_T}\right)(1 - \cos^2 4\Theta) - \left(\frac{\alpha^2}{32}\right)\left(\frac{C_L^2}{C_L - C_T}\right)(1 - \cos 4\Theta) - \left(\frac{\alpha\beta}{4}\right)\left(\frac{C_T C_L}{C_L - C_T}\right)(1 - \cos 4\Theta)\cos 2\Theta - \left(\frac{C'_{16} - C'_{26}}{2}\right)\sin 4\Theta \quad \text{(Eq 4)}$$

where the C'_{16} and C'_{26} values result from stress-induced symmetry distortion and the stress $T(\Theta)$ is

$$T = \frac{\sigma_a + \sigma_b}{2} + \frac{\sigma_a - \sigma_b}{2}\cos 2(\Omega - \Theta) \quad \text{(Eq 5)}$$

where Ω is the angle between the rolling direction and the direction of principal stress. This is a general solution to first order in stress-induced anisotropy and second order in textural anisotropy for plane-wave propagation in a biaxially stressed orthorhombic material. Neglect of higher-order terms in stress-induced anisotropy is justified for stresses in the range of engineering interest (i.e., stress levels insufficient to produce material failure).

Figure 4 defines the angles Θ and Ω as well as the principal stresses σ_a and σ_b for Eq 4 and 5. Other terms in these equations are defined as:

$$C_L = \frac{C'_{11} + C'_{22}}{2} \quad \text{(Eq 6a)}$$

$$C_T = C'_{66} \quad \text{(Eq 6b)}$$

$$\alpha = \frac{C'_{11} - C'_{22}}{C_L} \quad \text{(Eq 6c)}$$

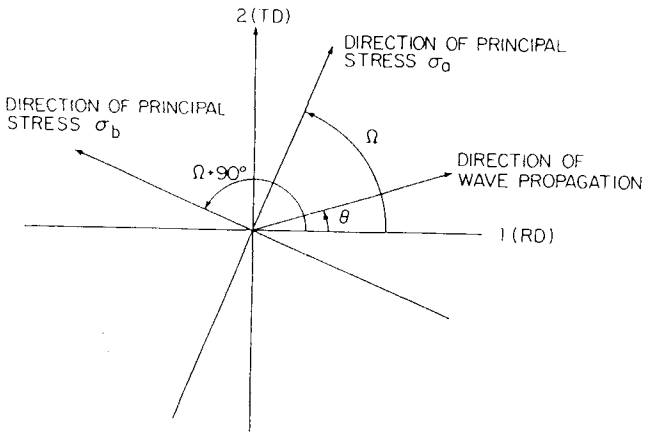

Fig. 4 Directions of wave propagation and stress in the 1-2 plane

$$\beta = \frac{\left(\frac{C_L - C'_{12}}{2}\right) - C_T}{C_T} \qquad \text{(Eq 6d)}$$

where α and β are measures of the longitudinal and shear-wave anisotropies, respectively. The C_{ij} are the conventional elastic constants in the state of interest with numerical subscripts in conventional notation (Ref 1) referring to the axes of Fig. 1(a). There are nine such independent elastic constants for orthorhombic symmetry. Sayers and Allen (Ref 16) have discussed the effect of stress fields on the conventional elastic constants and have shown that the C'_{ij} in a stressed material have a small but measurable difference from the C_{ij} of the same unstressed material. If the principal stress directions in an orthorhombic material are along the material symmetry directions, the number of independent elastic constants remains nine, but principal stresses off axes distort the orthorhombic symmetry to produce monoclinic symmetry with 14 independent elastic constants. The extra stress-induced constants, like the difference between C_{ij} and C'_{ij}, are small.

To accomplish the stress evaluation, V_T can be measured in two mutually orthogonal directions in the 1-2 plane, because it has been shown (Ref 4, 6-11) using Eq 4 and 5 that:

$$\frac{V_T(\Theta) - V_T(\Theta + 90°)}{(C_T/\rho)^{1/2}} = \left(\frac{\sigma_a - \sigma_b}{2C_T}\right)\cos 2(\Omega - \Theta) - \left(\frac{\alpha\beta}{8}\right)\left(\frac{C_L}{C_L - C_T}\right)(\cos 2\Theta - \varsigma\cos 6\Theta) \qquad \text{(Eq 7)}$$

The derivation of Eq 7 makes the reasonable assumption that texture-induced anisotropy is small, and only terms linear in σ, α, and β or quadratic in α and β are retained. The first term on the right-hand side of Eq 7 is directly proportional to stress. Biott (Ref 3) has noted that this term arises from a fundamental physical difference between the anisotropy generated in a medium by stress as compared to that generated by texture. Thurston (Ref 2) and MacDonald (Ref 17) have also discussed aspects of this term, and it has been emphasized (Ref 6) that the proportionality constant depends only on the linear elastic constant of the material and hence is not subject to the well-known strong influence of microstructure on nonlinear elastic properties.

The second term on the right-hand side of Eq 7 may be thought of as an error induced by textural anisotropy. When it is negligible, the principal stress difference may be deduced by varying Θ until the magnitude of the left-hand side is maximized and then setting that value equal to $(\sigma_a - \sigma_b)/2C_T$. If the

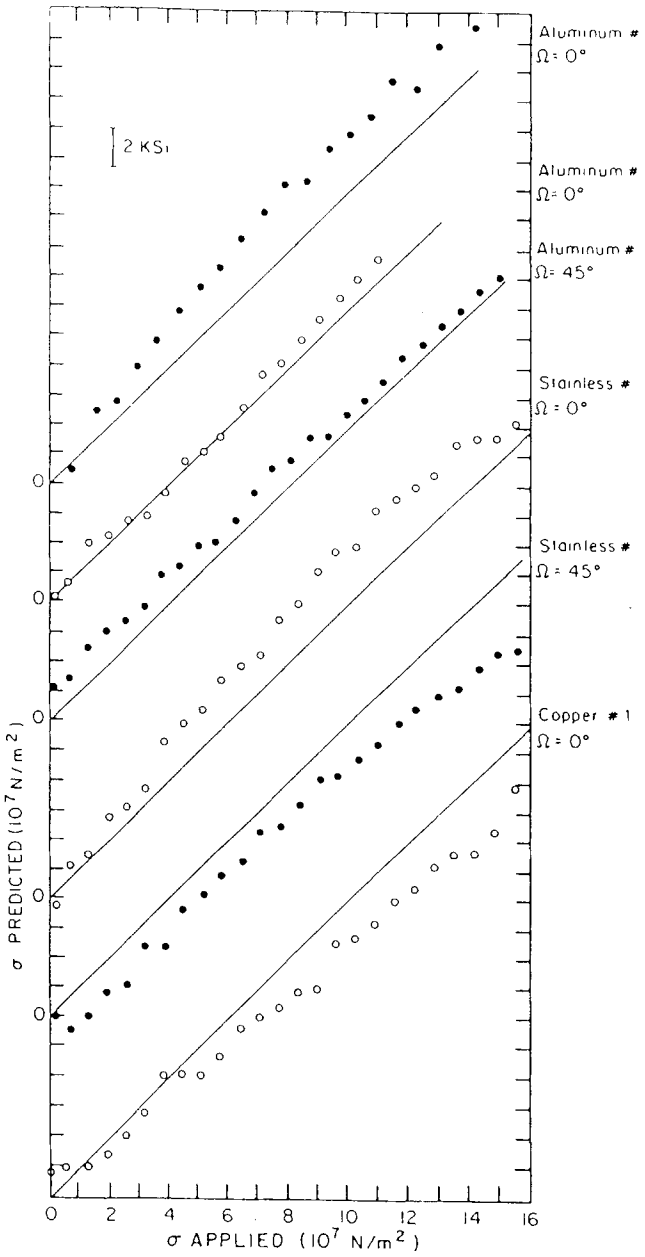

Fig. 5 Comparison of ultrasonically predicted stress (ordinate) with the actually applied stress (abscissa). The vertical and horizontal scales are the same, so perfect agreement would lie along the solid lines with 45° slope.

anisotropy term is not small, a procedure is still available for removing its influence on the data. Because Eq 7 contains only one term with a 6Θ angular variation and because that term has second-order material anisotropy parameters determining its coefficient, that coefficient can be evaluated from the values of the 6Θ term in a Fourier-series representation of $[V_T(\Theta) - V_T(\Theta + 90°)]$. The entire anisotropy term can then be subtracted from the data, and the foregoing procedure can be applied to the corrected data to deduce the principal stress difference independent of the texture-induced anisotropy in the elastic constants.

Stress prediction by the foregoing procedures has been tested on rolled sheets of cubic aluminum, stainless steel, and copper. The results are shown in Fig. 5, where predicted stress values from ultrasonic determination are plotted against the applied hydraulic tension. The plotted points are the experimental data. The scales of the ordinate and the abscissa are the same, so perfect fits would lie on the solid lines with 45° slope. The numerical parameters after the metal names represent different textures, and the Ω values represent the angular difference between the rolling direction and the applied stress. Testing has also been done on hexagonal metals, including titanium and zirconium alloys.

3. Measurement of Texture

The relation between texture and ultrasonic bulk wave velocities has been derived by Sayers et al. (Ref 18, 19), who considered the case of a polycrystalline aggregate composed of cubic single crystals. As justified above, the aggregate was assumed to have orthorhombic symmetry on the macroscale. In the Sayers model, the crystallite orientation distribution function (CODF) is used to describe the texture. The CODF gives the probability that a crystallite will have its axes at Euler angles, Θ, ψ, ϕ, with respect to the axes of Fig. 1(a). Textural information can be determined by extracting the anisotropy terms that were suppressed in the determination of stress. This can be accomplished by solving for the four elastic parameters, α, β, C_T, and C_L, defined in Eq 6(a) to (d). These parameters can be evaluated (Ref 9) from measurements of the velocities in Eq 8(a) to (d):

$$C_L = \frac{V_L^2(0°) + V_L^2(90°)}{2} - \frac{\sigma_a + \sigma_b}{2} \qquad \text{(Eq 8a)}$$

$$C_T = \frac{V_T^2(0°) + V_T^2(90°)}{2} - \frac{\sigma_a + \sigma_b}{2} \qquad \text{(Eq 8b)}$$

$$\alpha C_L = [V_L^2(0°) - V_L^2(90°)] - (\sigma_a - \sigma_b)\cos 2\Omega \qquad \text{(Eq 8c)}$$

$$\beta C_T = [V_T^2(45°) - V_T^2(0°)] + \left(\frac{\sigma_a - \sigma_b}{2}\right)(\cos 2\Omega - \sin 2\Omega) + \frac{(\alpha')^2}{16}\left(\frac{C_L^2}{C_L - C_T}\right) \qquad \text{(Eq 8d)}$$

If the material is unstressed, the solution is straightforward. Equations 8(a) and (b) may be first solved individually for C_L and C_T, which then allows resolution of α and β from Eq 8(c) and (d), respectively.

The values of the four elastic parameters can then be used to calculate the CODF, which quantifies the preferred orientation of the grains. For their polycrystalline aggregate, Sayers et al. (Ref 18, 19) expanded the CODF, $w(\xi,\psi,\phi)$, in a series of complex exponentials and Legendre functions, $Z_{lmn}(\xi)$, as defined by Roe (Ref 20-22):

$$w(\xi,\psi,\phi) = \sum_{l=0}^{\infty} \sum_{m=-l}^{l} \sum_{n=-l}^{l} W_{lmn}\, Z_{lmn}(\xi)\, e^{-im\psi}\, e^{-in\phi} \qquad \text{(Eq 9)}$$

Here, θ, ψ, and ϕ are the Euler angles with respect to the symmetry axes of the aggregate (Fig. 1a) and $\xi = \cos\theta$. The W_{lmn} are called the orientation distribution coefficients (ODCs).

Sayers et al. used a Voigt averaging scheme (Ref 23) to relate the effective second-order elastic moduli of the aggregate to the cubic single-crystal moduli (C_{11}^o, C_{12}^o, and C_{44}^o) and the ODCs. Symmetry arguments can be used to limit the number of ODCs. Bunge (Ref 24) indicates that for cubic crystallites some lower-order ODCs vanish; except for W_{000}, which is a normalization constant equal to $1/[4(2\Pi^2)]$, only three coefficients—W_{400}, W_{420}, and W_{440}—need be considered. Of these, W_{400} is insensitive to in-plane textural anisotropy. For aggregates of hexagonal crystallites (Ref 25, 26), W_{200} and W_{220} also need to be retained, with the number tending to increase with lower symmetry. The elastic moduli of the aggregate depend only on the ODCs, and thus the ultrasonic velocities of bulk, surface, and guided waves also depend on the ODCs.

Delsanto et al. (Ref 27, 28) have derived the relations between the velocities of surface waves and the ODCs for moderate texture, while Thompson and coworkers (Ref 11, 29) have related the ODCs to the velocities of the lowest-order plate shear-horizontal wave and symmetrical Lamb wave modes (Ref 30). The latter results for waves propagating at an angle Θ from the rolling direction are, to the first order in the elastic anisotropy:

$$V_{SH_o}(\Theta) = \left(\frac{\hat{C}_T}{\rho}\right)^{1/2}\left[1 + \left(\frac{\hat{\beta}}{4}\right)(1 - \cos 4\Theta) + \ldots\right] \qquad \text{(Eq 10a)}$$

$$V_{S_o}(\Theta) = \left(\frac{\hat{C}_L}{\rho}\right)^{1/2}\left[1 + \left(\frac{\hat{\alpha}}{4}\right)\cos 2\Theta - \left(\frac{C_T}{4C_L}\right)(1 - \cos 4\Theta) + \ldots\right] \qquad \text{(Eq 10b)}$$

The velocity V_{SH_o} refers to the horizontally polarized shear mode, and the velocity V_{S_o} refers to the lowest-order symmetrical Lamb mode. Here the circumflex (^) is used to indicate parameters appropriate to guided-wave rather than plane-wave propagation. These velocities are relatively easily measured (Ref 31) with electromagnetic acoustic transducers (EMAT)

Table 1 Comparison of Voigt, Reuss, and Hill average values for the CODF expansion coefficients of four different materials as evaluated from S_0 and SH_0 Lamb waves

CODF expansion coefficient	1100 Al	629 °F Al	675 °F Al	Copper
$W_{440}(SH_o)_V$	–0.00573	0.00505	0.00303	–0.00303
$W_{440}(SH_o)_R$	–0.00555	0.00489	0.00294	–0.00334
$W_{440}(SH_o)_H$	–0.00564	0.00497	0.00298	–0.00318
$W_{440}(S_o)_V$	–0.00581	0.00551	0.00296	–0.00304
$W_{440}(S_o)_R$	–0.00564	0.00535	0.00287	–0.00342
$W_{440}(S_o)_H$	–0.00572	0.00543	0.00291	–0.00322
$W_{420}(S_o)_V$	–0.00008	–0.00403	–0.00265	0.00121
$W_{420}(S_o)_R$	–0.00008	–0.00389	–0.00257	0.00123
$W_{420}(S_o)_H$	–0.00008	–0.00396	–0.00262	0.00122
$W_{400}(SH_o)_V$	–0.04521	–0.06566	–0.05482	0.04213
$W_{400}(SH_o)_R$	–0.05922	–0.07904	–0.06853	–0.05082
$W_{400}(SH_o)_H$	–0.05232	–0.07245	–0.06178	–0.00203
$W_{400}(S_o)_V$	–0.00791	0.01378	–0.00867	–0.01247
$W_{400}(S_o)_R$	–0.01175	0.00849	–0.01319	–0.01272
$W_{400}(S_o)_H$	–0.00986	0.01109	–0.01097	–0.00008

(Ref 32). The parameters $\hat{\alpha}$ and $\hat{\beta}$ describe the anisotropy of guided modes and can be related to the velocities of Eq 10(a) and (b):

$$\hat{\alpha} = \frac{2[V_{S_o}(0°) - V_{S_o}(90°)]}{(\hat{C}_L/\rho)} \quad \text{(Eq 11a)}$$

$$\hat{\beta} = \frac{2[V_{SH_o}(45°) - V_{SH_o}(0°)]}{(\hat{C}_T/\rho)} \quad \text{(Eq 11b)}$$

In one approach, the plane-wave parameters, C_L, C_T, α, and β, can be used in the evaluation of the CODFs. These can be derived from measurements in the plate material by the following relationships:

$$\hat{C}_L = C_L - \frac{P^2 - (2^{1/2})(32/35)\pi^2 C^o P(1 + P/L)W_{400}}{L} \quad \text{(Eq 12a)}$$

$$\hat{C}_T = C_T \quad \text{(Eq 12b)}$$

$$\hat{\alpha} = \alpha\left[\frac{1 + (2P/L)}{1 - (P^2L^2)}\right] \quad \text{(Eq 12c)}$$

$$\hat{\beta} = \beta \quad \text{(Eq 12d)}$$

where the values capped with a circumflex denote measurements in plate material and the uncapped values represent the corresponding plane-wave measurements. The Voigt average isotropic moduli that appear in these equations are: $L = C^o_{11} - 2C^o/5$; $P = C^o_{12} + C^o/5$; $M = C^o_{44} + C^o/5$; where C^o is the elastic anisotropy $C^o = C^o_{11} - C^o_{12} - 2C^o_{44}$. The superscript ° indicates that the values are the single-crystal elastic constants.

The final step in the evaluation of the ODCs in this scenario is from the following relations:

$$C_L = L + \left[\frac{(2^{1/2})12\pi^2 C^o}{35}\right]\left[W_{400} + \left\{\frac{(70)^{1/2}}{3}\right\}W_{440}\right] \quad \text{(Eq 13a)}$$

$$C_T = M + \left[\frac{(2^{1/2})4\pi^2 C^o}{35}\right]\left[W_{400} - (70)^{1/2}W_{440}\right] \quad \text{(Eq 13b)}$$

$$\alpha = \frac{-(5^{1/2})32\pi^2 C^o W_{420}}{35L} \quad \text{(Eq 13c)}$$

$$\beta = \frac{(35)^{1/2}\, 16\pi^2 C^o W_{440}}{35M} \quad \text{(Eq 13d)}$$

With the ODCs evaluated from Eq 13(a) to (d), a CODF can be constructed and used to generate pole figures or other quantitative measures of the textural anisotropy. Equations have also been reported (Ref 33) which directly give the W_{4m0} in terms of the measured plate-wave velocities.

Textures from ultrasonic measurements have been determined (Ref 33-35) both for specimens of aluminum with three different textures and for a specimen of copper. For the textural analyses, a small correction (Ref 33) to the V_{S_o} velocities was made for dispersion effects. The initial texture analyses were done with Voigt averaging (Ref 23), but Hirao et al. (Ref 36) have questioned the use of such averaging rather than Reuss (Ref 37) or Hill (Ref 38) averaging. Voigt averaging assumes homogeneous strain in a polycrystalline aggregate and averages over stress, whereas Reuss averaging assumes homogeneous stress and averages over strain. Hill averaging compromises as an arithmetic mean of the other two averages.

The textures from the aluminum and copper data were therefore determined with all three averages. The results are compared in Table 1, which lists W_{4m0} values. It may be noted that W_{440} and W_{400} are overdetermined, with values derived from both SH_o and S_o modes, while determination of W_{420} can be

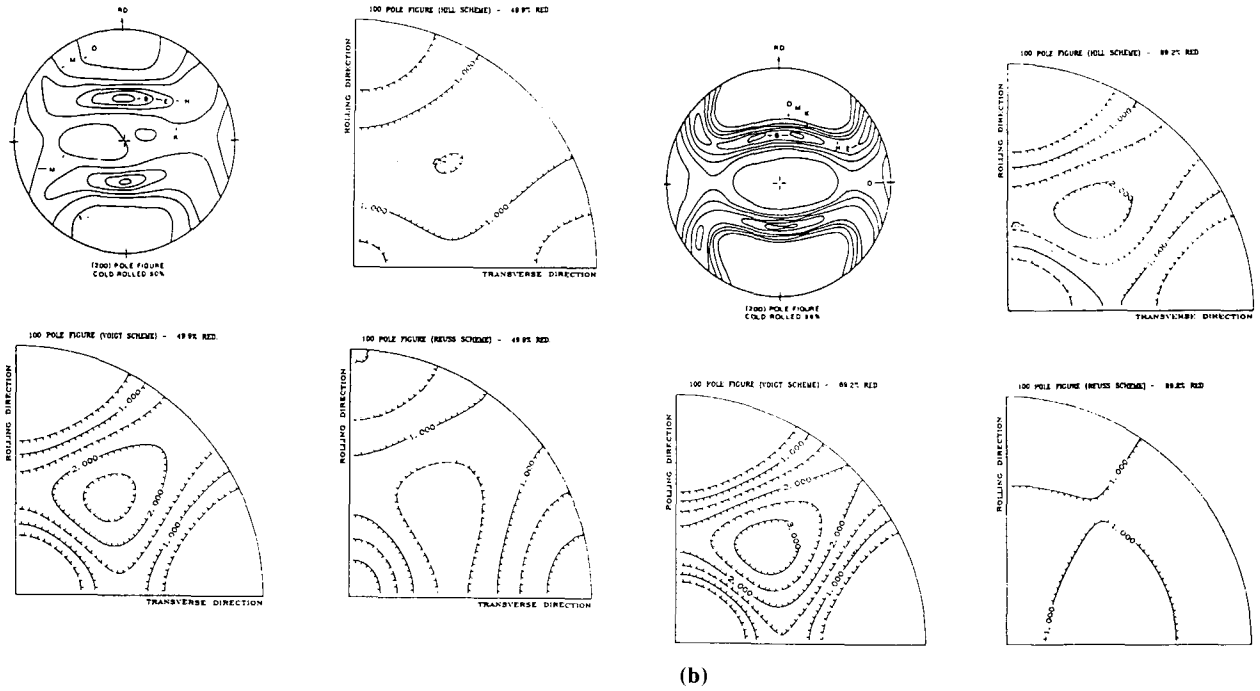

Fig. 6 Comparisons of x-ray pole figures with ultrasonically determined pole figures using Hill averaging, Voigt averaging, and Reuss averaging. (a) Rolled copper with 50% reduction. (b) Rolled copper with 89% reduction

Table 2 Comparison of Hill averages of CODF expansion coefficients from ultrasonic data with expansion coefficients from x-ray or neutron diffraction data

CODF expansion coefficient	1100 Al	629 °F Al	678 °F Al	Copper
		Ultrasonic data		
$W_{440}(SH_o)_H$	–0.00564	0.00497	0.00298	–0.00318
$W_{440}(S_o)_H$	–0.00572	0.00543	0.00291	–0.00322
$W_{420}(S_o)_H$	–0.00008	–0.00396	–0.00262	0.00122
$W_{400}(SH_o)_H$	–0.05232	–0.07245	–0.06178	–0.00203
$W_{400}(S_o)_H$	–0.00986	0.01109	–0.01097	–0.00008
	X-ray(a)	Neutron(b)	Neutron(b)	X-ray(b)
W_{440}	–0.00472	0.0069	0.0043	–0.00432
W_{420}	–0.00028	–0.0034	–0.0033	0.00132
W_{400}	0.00098	0.0097	0.0078	0.00113

(a) X-ray diffraction evaluation from G.C. Johnson, University of California—Berkeley. (b) Neutron diffraction evaluation from G.V. Blessing and R.C. Reno, National Bureau of Standards

done only with S_o modes. In most instances differences are on the order of 10 to 20%, with agreement in the case of W_{400} tending to be least good. The poor agreement for W_{400} has been explained in terms of the requirements for absolute rather than relative velocity data and the strong dependence on the isotropic parameters. Textures for the same specimens were also determined by x-ray and neutron diffraction. The ODCs from the ultrasonic measurements are compared with the x-ray and neutron diffraction results in Table 2.

Comparisons (Ref 35) of ultrasonic and x-ray pole figures for copper at two levels of rolling reduction are shown in Fig. 6(a) and (b). The ultrasonic pole figures were done with all three types of averaging; the pole figures from Hill averaging (Ref 38) show the best agreement with x-ray pole figures. The symmetries of all ultrasonic pole figures parallel the symmetry of the corresponding x-ray pole figure, although in fairness it must be acknowledged that the pole figure from Reuss averaging for the 89% reduction of copper shows very little detail. Conversely, one must question how much of the x-ray pole figure is really typical of the bulk texture as compared to the surface texture. Preliminary studies in the hexagonal metals titanium and zirconium have also been reported (Ref 39-41).

4. Applications

An important consequence of texture is its influence on plastic deformability, and use of ultrasonic measurements to

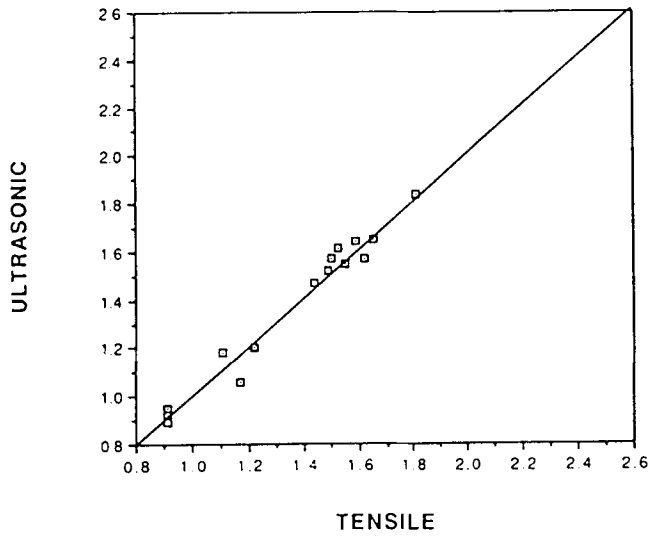

Fig. 7 Comparison of ultrasonic and tensile measurements of $\bar{r}$ from a set of samples provided by the Wheeling Pittsburgh and Weirton steel companies. Ultrasonic predictions utilize the correlations of Mould and Johnson. (Ref 47)

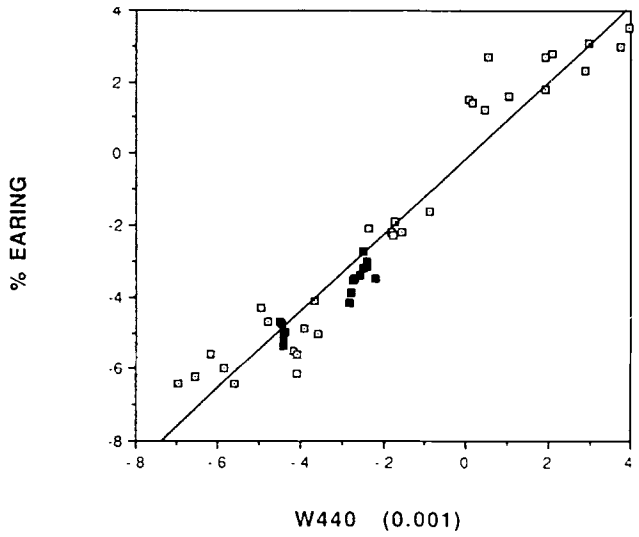

Fig. 8 Fourfold earing versus W_{440} as measured on 3004 aluminum alloy with SH waves (open data points) and on 3104-H10 aluminum alloy with S_0 waves (closed data points)

obtain relevant textural information has been the subject of recent studies (Ref 42-44). In steel, W_{400} is known to correlate with the average normal anisotropy (or plastic strain ratio), $\bar{r}$, a parameter used to predict the ability of a material to withstand deep-drawing operations. Several investigators have demonstrated the prediction of $\bar{r}$ from ultrasonic measurements, with Fig. 7 illustrating one example. In the production of aluminum beverage cans, a primary concern is the formation of "ears" (scalloping around the top of the can). Figure 8 presents a plot showing the correlation of W_{440}, as determined ultrasonically, with the degree of fourfold earing (Ref 45). Further work has been concerned with the measurement of the Kearns f-parameters in zircaloy (Ref 46). These measurements describe the effective fraction of basal poles aligned along symmetry directions and are important in describing the mechanical properties in nuclear applications.

5. Conclusions

Anisotropies in the ultrasonic velocities can be produced by either stress or texture. Schemes are reported, based on the angular dependence of wave speeds, which allow these two sources of anisotropy to be independently determined and quantitatively evaluated. Experimental results have demonstrated the ability to make quantitative predictions of the orientation distribution coefficients and to use this information in the quantitative prediction of formability parameters.

References

1. C. Kittel, *Introduction to Solid State Physics*, 2nd ed., John Wiley & Sons, 1956, chap IV
2. R.N. Thurston, *J. Acoust. Soc. Am.*, Vol 37, 1965, p 348
3. M.A. Biott, *J. Appl. Phys.*, Vol 11, 1940, p 522
4. R.B. Thompson, S.S. Lee, and J.F. Smith, *J. Acoust. Soc. Am.*, Vol 80, 1986, p 921
5. J.F. Smith and J.D. Greiner, *J. Met.*, Vol 32, 1980, p 34
6. R.B. Thompson, J.F. Smith, and S.S. Lee, in *Nondestructive Evaluation: Applications to Materials Processing*, O. Buck and S. Wolf, Ed., American Society for Metals, 1984, p 155
7. R.B. Thompson, J.F. Smith, and S.S. Lee, in *Review of Progress in Quantitative Nondestructive Evaluation*, Vol 2B, D.O. Thompson and D.E. Chimenti, Ed., Plenum Press, 1983, p 1339
8. R.B. Thompson, J.F. Smith, and S.S. Lee, *Appl. Phys. Lett.*, Vol 44, 1984, p 296
9. R.B. Thompson, S.S. Lee, and J.F. Smith, in *Review of Progress in Quantitative Nondestructive Evaluation*, Vol 3B, D.O. Thompson and D.E. Chimenti, Ed., Plenum Press, 1984, p 1311
10. S.S. Lee, J.F. Smith, and R.B. Thompson, in *Review of Progress in Quantitative Nondestructive Evaluation*, Vol 4B, D.O. Thompson and D.E. Chimenti, Ed., Plenum Press, 1985, p 1061
11. R.B. Thompson, J.F. Smith, and S.S. Lee, in *In Process Nondestructive Evaluation and Process Control*, H. Wadley, Ed., American Society for Metals, 1986, p 73
12. T. Tokuoka and Y. Iwashimizu, *Int. J. Solids Struct.*, Vol 4, 1968, p 383
13. R.B. King and C.M. Fortunko, *J. Appl. Phys.*, Vol 54, 1983, p 3027
14. R.B. King and C.M. Fortunko, *Ultrasonics*, Vol 21, 1983, p 256
15. C.S. Man and W.Y. Lu, *J. Elasticity*, Vol 17, 1987, p 159
16. C.M. Sayers and D.R. Allen, *J. Phys. D. Appl. Phys.*, Vol 17, 1984, p 1399
17. D.E. MacDonald, *IEEE Trans. Sonics Ultrasonics*, Vol SU-28, 1981, p 75
18. C.M. Sayers, *J. Phys. D. Appl. Phys.*, Vol 15, 1982, p 2157
19. D.R. Allen, R. Langman, and C.M. Sayers, *Ultrasonics*, Vol 23, 1985, p 215
20. R.J. Roe, *J. Appl. Phys.*, Vol 37, 1966, p 2069
21. R.J. Roe and W.R. Krigbaum, *J. Chem. Phys.*, Vol 40, 1964, p 2608
22. R.J. Roe, *J. Appl. Phys.*, Vol 36, 1965, p 2024
23. W. Voigt, *Lehrbuch der Kristallphysik*, Taubner, Leipzig, 1928, p 962
24. H.J. Bunge, *Kristall. Tech.*, Vol 3, 1968, p 431
25. C.M. Sayers, *Ultrasonics*, Vol 24, 1986, p 289
26. Y. Li and R.B. Thompson, *J. Appl. Phys.*, Vol 67, 1990, p 2663

27. P.P. Delsanto and A.V. Clark, *J. Acoust. Soc. Am.*, Vol 26, 1988, p 188
28. P.P. Delsanto, R.B. Mignogna, and A.V. Clark, in *Proc. 2nd Int. Symp. Nondestructive Characterization of Materials*, J.F. Bussiere, Ed., Plenum Press, 1987, p 535
29. R.B. Thompson, S.S. Lee, and J.F. Smith, *Ultrasonics*, Vol 25, 1987, p 133
30. B.A. Auld, *Acoustic Waves and Fields in Solids*, Wiley-Interscience, 1973, chap. IX
31. S.S. Lee, J.F. Smith, and R.B. Thompson, in *Formability and Metallurgical Structure*, A.K. Sachdev and J.D. Embury, Ed., TMS-AIME, 1987, p 177
32. R.B. Thompson, in *Physical Acoustics*, Vol XIX, R.N. Thurston and L. Pierce, Ed., Academic Press, 1990, p 157
33. R.B. Thompson, J.F. Smith, S.S. Lee, and G.C. Johnson, *Metall. Trans. A*, Vol 20A, 1989, p 2431
34. A.V. Clark, Jr., R.C. Reno, R.B. Thompson, J.F. Smith, G.V. Blessing, R.J. Fields, P.P. Delsanto, and R.B. Mignona, *Ultrasonics*, Vol 26, 1988, p 189
35. J.F. Smith, Y. Li, and R.B. Thompson, in *Review of Progress in Quantitative Nondestructive Evaluation*, Vol 7B, D.O. Thompson and D.E. Chimenti, Ed., Plenum Press, 1988, p 1383
36. M. Hirao, K. Aoki, and H. Fukuoka, *J. Acoust. Soc. Am.*, Vol 81, 1987, p 1434
37. A. Reuss, *Z. Angew. Math. Mech.*, Vol 9, 1929, p 49
38. R. Hill, *Proc. R. Soc. (London) A*, Vol 65, 1952, p 349
39. S.S. Lee, B.Y. Ahn, H.J. Kim, and Y.C. Kim, in *Nondestructive Characterization of Materials IV*, C.O. Ruud, J.F. Bussiere, and R.E. Green, Jr., Ed., Plenum Press, 1990, p 439
40. Y. Li, R.B. Thompson, J.H. Rose, and T.M. Holden, in *Nondestructive Characterization of Materials IV*, C.O. Ruud, J.F. Bussiere, and R.E. Green, Jr., Ed., Plenum Press, 1990, p 467
41. Y. Li, S.S. Lee, R.B. Thompson, and C.M. Sayers, *Mater. Sci. Eng. A*, Vol A177, 1994, p 761
42. M. Hirao, H. Fukuoka, K. Fujisawa, and R. Murayama, *J. Nondestr. Eval.*, Vol 12, 1993, p 27
43. R.B. Thompson, E.P. Papadakis, D.D. Bluhm, G.A. Alers, K. Forouraghi, H.D. Skank, and S.J. Wormley, *J. Nondestr. Eval.*, Vol 12, 1993, p 45
44. K. Kawashima, T. Hyoguchi, and T. Akagi, *J. Nondestr. Eval.*, Vol 12, 1993, p 71
45. R.B. Thompson, Progress in the Ultrasonic Characterization of Texture and Formability of Rolled Metal Sheets, *Mater. Eval.*, Vol 51, 1993, p 1162
46. R.B. Thompson, A.J. Anderson, and C.S. Cook, in *Nondestructive Characterization of Materials VI*, R.E. Green, Jr., T. Kishi, M.H. Manghnani, and C.O. Ruud, Ed., Plenum Press, in press
47. P.R. Mould and T.E. Johnson, *Sheet Met. Ind.*, 1973, p 328